

Direct collapse to supermassive black hole seeds: the critical conditions for suppression of H₂ cooling

Yang Luo,^{1*} Isaac Shlosman,^{2,3} Kentaro Nagamine^{3,4,5} and Taotao Fang¹

¹*Department of Astronomy and Institute of Theoretical Physics and Astrophysics, Xiamen University, Xiamen, Fujian 361005, China*

²*Department of Physics & Astronomy, University of Kentucky, Lexington, KY 40506-0055, USA*

³*Theoretical Astrophysics, Department of Earth & Space Science, Osaka University, 1-1 Machikaneyama, Toyonaka, Osaka 560-0043, Japan*

⁴*Department of Physics & Astronomy, University of Nevada, Las Vegas, NV 89154-4002, USA*

⁵*Kavli-IPMU (WPI), University of Tokyo, 5-1-5 Kashiwanoha, Kashiwa, Chiba, 277-8583, Japan*

Accepted XXX. Received YYY; in original form ZZZ

ABSTRACT

Observations of high-redshift quasars imply the presence of supermassive black holes (SMBHs) already at $z \sim 7.5$. An appealing and promising pathway to their formation is the direct collapse scenario of a primordial gas in atomic-cooling haloes at $z \sim 10 - 20$, when the H₂ formation is inhibited by a strong background radiation field, whose intensity exceeds a critical value, J_{crit} . To estimate J_{crit} , typically, studies have assumed idealized spectra, with a fixed ratio of H₂ photo-dissociation rate k_{H_2} to the H⁻ photo-detachment rate k_{H^-} . This assumption, however, could be too narrow in scope as the nature of the background radiation field is not known precisely. In this work we argue that the critical condition for suppressing the H₂ cooling in the collapsing gas could be described in a more general way by a combination of k_{H_2} and k_{H^-} parameters, without any additional assumptions about the shape of the underlying radiation spectrum. By performing a series of cosmological zoom-in simulations covering a wide range of relevant k_{H_2} and k_{H^-} parameters, we examine the gas flow by following evolution of basic parameters of the accretion flow. We test under what conditions the gas evolution is dominated by H₂ and/or atomic cooling. We confirm the existence of a critical curve in the $k_{\text{H}_2} - k_{\text{H}^-}$ plane, and provide an analytical fit to it. This curve depends on the conditions in the direct collapse, and reveals domains where the atomic cooling dominates over the molecular cooling. Furthermore, we have considered the effect of H₂ self-shielding on the critical curve, by adopting three methods for the effective column density approximation in H₂. We find that the estimate of the characteristic lengthscale for shielding can be improved by using $\lambda_{\text{Jeans}25}$, which is 0.25 times that of the local Jeans length, which is consistent with previous one-zone modeling.

Key words: methods: numerical — galaxies: formation — galaxies: high-redshift — cosmology: theory — cosmology: dark ages, reionization, first stars — quasars: supermassive black holes

1 INTRODUCTION

Supermassive black holes (SMBHs) with masses of $\sim 10^9 M_{\odot}$ have been found in the less than 750 Myr-old universe, at $z \sim 7.5$, in the midst of quasars (Fan et al. 2003; Mortlock et al. 2011; Willott et al. 2010; Wu et al. 2015; Venemans et al. 2017; Bañados et al. 2018). The origin of these SMBHs is still an open question, and it is not clear how they have managed to grow so quickly after the Big Bang.

The SMBH seeds can in principle grow via supercritical accretion from stellar mass black holes — the end products of metal-free Population III stars (e.g., Madau et al. 2014; Lupi et al. 2016; Li & Cao 2019). But this growth rate requires a massive reservoir of accretion matter feeding the Pop III remnant over long time intervals, e.g., longer than 100 Myr (e.g., Begelman et al. 2006; Tanaka & Haiman 2009). Such an option can be realized in the form of a supermassive star (Volonteri & Rees 2006; Begelman 2010), but its existence must be verified in the first place. Another possibility is the runaway collapse of compact stellar clusters,

* E-mail: yangluo@xmu.edu.cn (YL)

subject to general relativistic effects (Zel'dovich & Podurets 1965; Shapiro & Teukolsky 1985), or stellar/gas dynamical evolution of stellar clusters (Begelman & Rees 1978; Lupi et al. 2014). Their existence at high redshifts is difficult to explain, and their collapse imposes additional conditions on properties of their stellar and gaseous components.

One of the most promising ways to form the SMBH seeds at high redshifts is the direct collapse scenario, which involves the baryonic collapse within dark matter (DM) haloes (e.g., Rees 1984; Haehnelt & Rees 1993; Loeb & Rasio 1994; Bromm & Loeb 2003; Koushiappas et al. 2004; Begelman et al. 2006). In the direct collapse, the virial temperature of DM haloes must exceed the cooling floor of the primordial gas, and the seed black holes as massive as $\sim 10^4 - 10^6 M_\odot$ can form. The direct collapse paradigm requires that the gas remains atomic to avoid fragmentation, and the high inflow rate is maintained. Furthermore, the infalling gas has to overcome the angular momentum barrier (Begelman & Shlosman 2009).

Numerical modeling of an optically-thin phase of a direct collapse has been performed and confirmed previous theoretical estimates. The collapsing gas must be prevented from forming molecular hydrogen (e.g. Shang et al. 2010; Latif et al. 2013) to avoid fragmentation and formation of the Pop III stars (e.g. Haiman et al. 2000; Bromm & Loeb 2003; Wise & Abel 2008; Regan & Haehnelt 2009; Greif et al. 2011; Choi et al. 2013, 2015; Shlosman et al. 2016; Latif et al. 2013, 2016).

Suppression of the H_2 cooling requires the presence of a strong ultraviolet (UV) background radiation field, which can dissociate H_2 . In most studies, the minimum value of the UV intensity to suppress the H_2 cooling is denoted by J_{crit} , in units of $J_{\text{LW},21} = 10^{-21} \text{ erg s}^{-1} \text{ cm}^{-2} \text{ Hz}^{-1} \text{ sr}^{-1}$. The UV background intensity in the early universe is expected to come from the cosmic star formation (e.g., Greif et al. 2007; Haardt & Madau 2012). Subsequent analysis has indicated that the background intensity may not be strong enough to reach the required J_{crit} (e.g. Ciardi et al. 2000; Ciardi & Ferrara 2005; Dijkstra et al. 2008; Ahn et al. 2009; Holzbauer & Furlanetto 2012).

To assure that the collapsing gas within a DM halo will be able to follow the isothermal track, it was claimed that the direct collapse haloes must be located close to the star-forming galaxies (e.g., Agarwal et al. 2012; Dijkstra et al. 2014), or follow synchronized collapse within two haloes at a small separation (Visbal et al. 2014), in order to be subject to a strong UV flux. However, attempts to search for such haloes and obtain their population have encountered extreme difficulties (e.g., Yue et al. 2013; Chon & Latif 2017; Habouzit et al. 2016). The estimate of the number density of direct collapse haloes at $z \sim 10$ exposed to radiation from a nearby starforming galaxy is very sensitive to J_{crit} (e.g., Dijkstra et al. 2008; Agarwal et al. 2012; Dijkstra et al. 2014; Yue et al. 2014; Inayoshi & Tanaka 2015; Yue et al. 2017; Maio et al. 2019). A variation by an order of magnitude in J_{crit} can lead to the five orders of magnitude variation in this probability. This emphasizes the need to obtain a more stringent constraint on the value of J_{crit} and on the uncertainties in its determination.

The value of J_{crit} is strongly dependent on the background radiation spectral shape. To suppress the H_2 cooling, the H_2 fraction could be reduced by the H^- photo-

detachment, as an alternative mechanism to the H_2 photo-dissociation. Hence, the value of J_{crit} depends on the relative contribution from H^- photo-detachment rate, k_{H^-} , and from H_2 photo-dissociation rate, k_{H_2} (e.g., Sugimura et al. 2014). For a given radiation spectral shape, k_{H^-} and k_{H_2} can be calculated from

$$k_{H^-} = \alpha \kappa_{H^-} J_{\text{LW}} \quad (1)$$

$$k_{H_2} = \beta \kappa_{H_2} J_{\text{LW}}, \quad (2)$$

where $\kappa_{H^-} \approx 1.1 \times 10^{-10} \text{ s}^{-1}$ and $\kappa_{H_2} \approx 1.38 \times 10^{-12} \text{ s}^{-1}$ are the rate coefficients of H^- photo-detachment and H_2 photo-dissociation, respectively (e.g., Abel et al. 1997; Glover & Jappsen 2007; Miyake et al. 2010). Dimensionless parameters α and β provide the dependence on the radiation spectral shape (Glover & Jappsen 2007). When the specific intensity at 13.6 eV becomes larger than J_{crit} , the H_2 cooling can be inhibited.

In most cases, the estimate of J_{crit} is obtained by assuming a particular spectral shape, either a blackbody or a power law. To be representative of dominant Pop III stellar populations in galaxies, the radiation field has been modeled as a blackbody with $T_\star = 10^5 \text{ K}$, hereafter referred to as T5 (Omukai 2001; Shang et al. 2010; Hartwig et al. 2015a; Inayoshi & Tanaka 2015). On the other hand, for stellar populations dominated by the Pop II stars, the blackbody with $T_\star = 10^4 \text{ K}$ (i.e., T4) has been used (Omukai 2001; Shang et al. 2010; Latif et al. 2014; Inayoshi & Tanaka 2015). More realistic spectral shapes can contain a mixture of various stellar populations, and sources with power-law spectra cannot be ruled out either.

The values of J_{crit} , in units of $J_{\text{LW},21}$, obtained in previous studies span a large range, from as low as 20 to as high as 10^5 , depending on the incident radiation spectral shape, and the treatment of the H_2 self-shielding (e.g. Wolcott-Green et al. 2011; Sugimura et al. 2014; Hartwig et al. 2015a; Agarwal et al. 2016; Wolcott-Green et al. 2017; Dunn et al. 2018).

For the T5 and T4 blackbody spectra, the ratio of k_{H^-} to k_{H_2} is fixed. However, realistically, the background radiation spectrum is expected to evolve, and hence both k_{H^-} and k_{H_2} will be changing with time. The hardness of radiation spectra of starforming galaxies will evolve as well, and thus its contribution to the H_2 dissociation rate (Leitherer et al. 1999; Schaerer 2003; Inoue 2011; Sugimura et al. 2014; Visbal et al. 2015; Agarwal et al. 2016). Moreover, trapping of Ly α photons emitted in an optically-thick accretion flow during the direct collapse can affect the gas cooling (e.g., Schleicher et al. 2010; Ge & Wise 2017), and even photo-detach most of H^- (e.g., Johnson & Dijkstra 2017). Under these conditions, the ratio of k_{H^-} to k_{H_2} cannot be calculated simply.

Additionally, the value of J_{crit} depends on the treatment of H_2 self-shielding (Wolcott-Green et al. 2011; Hartwig et al. 2015a). With higher H_2 density, the gas becomes optically-thick to the UV radiation, and can be self-shielded from the background radiation. Most numerical simulations used the local Jeans length to calculate the column densities for self-shielding, but this assumption can lead to an overestimate of J_{crit} (e.g., Wolcott-Green et al. 2011). In three-dimensional (3D) simulations, the self-shielding depends on the direction as well, due to a spatial variation of the gas density and its temperature. This directional depen-

dence can cause a substantial difference in the estimate of J_{crit} , between 3D and one-zone simulations (e.g., Shang et al. 2010). Additional effects, such as shock capturing and hydrodynamical effects, can become important in 3D simulations, as have been suggested (e.g., Latif et al. 2014). Moreover, the X-rays could increase the hydrogen ionization fraction and the free electron fraction, which promotes the H⁻ and H₂ formation via the electron-catalysed reactions (see Equations 3 and 4). The effect of extragalactic X-ray background could increase the value of J_{crit} by a factor of 3 to 10, depending on the spectral shape of the background UV radiation (Inayoshi & Haiman 2014; Latif et al. 2015; Glover 2016). Other uncertainties, like chemical reactions (Glover 2015a), the rate coefficient of the collisional ionization of hydrogen (Glover 2015b), and anisotropy in the external radiation (Regan et al. 2016) could also introduce an uncertainty of up to a factor of 5 into the determination of J_{crit} .

The critical intensity lacks a unique value, and can be determined by a combination of k_{H^-} and k_{H_2} , on a two-dimensional plane. For a given k_{H^-} , a critical value of k_{H_2} is expected to exist, above which the H₂ cooling will be suppressed. A critical curve has been found in the k_{H^-} and k_{H_2} plane for one-zone simulations (Agarwal et al. 2016; Wolcott-Green et al. 2017). This curve provides a more general way of determining the critical conditions, without any assumptions of the shape of the underlying radiation spectrum. But a question remains about the existence of such a curve in 3D simulations. How does the critical curve depend on the spatial variations in the density and temperature in 3D? How does the critical curve from 3D hydrodynamic simulations compares to those obtained from one-zone modeling? What is the effect of the H₂ self-shielding approximation on the shape of this curve? In this work, we investigate the dependence of J_{crit} in the 3D cosmological zoom-in simulations on the H₂ self-shielding modeling and incident spectral shape, as given by k_{H^-} and k_{H_2} parameters.

This paper is structured as follows. Section 2 describes the numerical methods used here, the initial cosmological conditions, and chemical network for the molecular gas. Our results are presented in Section 3. Finally, we discuss and summarize this work in Section 4.

2 NUMERICAL METHOD

For simulations of direct collapse within DM haloes, we perform 3D zoom-in cosmological simulations using the Eulerian adaptive mesh refinement (AMR) code Enzo-2.5 (Bryan & Norman 1997; Norman & Bryan 1999; Bryan et al. 2014). To calculate the gravitational dynamics, a particle-mesh N -body method is implemented (Colella & Woodward 1984; Bryan et al. 1995). The hydrodynamics equations are solved by the piece-wise parabolic solver which is an improved form of the Godunov method (Colella & Woodward 1984). It makes use of the particle mesh technique to solve the DM dynamics and the multi-grid Poisson solver to compute the gravity. For more details of our simulations, we refer the reader to Luo et al. (2016), Luo et al. (2018) and Ardaneh et al. (2018).

2.1 Initial conditions

We use fully cosmological initial conditions (ICs) for our models and invoke zoom-in simulations (e.g. Choi et al. 2015; Luo et al. 2016; Shlosman et al. 2016; Luo et al. 2018; Ardaneh et al. 2018).

For the initial conditions, we adopt the MUSIC algorithm (Hahn & Abel 2011), which uses a real-space convolution approach in conjunction with an adaptive multi-grid Poisson solver to generate highly accurate nested density, particle displacement, and velocity fields suitable for multi-scale zoom-in simulations of structure formation in the universe. First, we generate $1 h^{-1}$ Mpc comoving with root grid 128^3 DM-only ICs, initially at $z = 199$, and run it without AMR until $z = 10$. Using the HOP group finder (Eisenstein & Hut 1998), we select three haloes with viral temperature above the cooling floor of the primordial gas. Then, we generate a zoom-in DM halo with 1024^3 effective resolution in DM and gas, centered on the selected halo position.

The zoom-in region is set to be large enough to cover the initial positions of all selected halo particles. For the DM particles in the zoom-in region, we use 10,223,616 particles which yield an effective DM resolution of about $99 M_{\odot}$. The baryon resolution is set by the size of the grid cells.

The grid cells are adaptively refined based on the following three criteria: baryon mass, DM mass and Jeans length. A region of the simulation grid is refined by a factor of 2 in length scale, if the gas or DM densities become greater than $\rho_0 2^{\alpha l}$, where ρ_0 is the density above which the refinement occurs, l is the refinement level. We set the ENZO parameter *MinimumMassForRefinementExponent* α to -0.2 , which reduces the threshold for refinement as higher densities are reached.

We have imposed the condition of at least 16 cells per Jeans length in our simulations, so that no artificial fragmentation would take place (Truelove et al. 1997). In all simulations, we set the maximum refinement level to 15, which is about $0.23 h^{-1}$ pc comoving.

We use the Planck 2015 for cosmology parameters (Planck Collaboration et al. 2016): $\Omega_m = 0.3089$, $\Omega_{\Lambda} = 0.6911$, $\Omega_b = 0.04859$, $\sigma_8 = 0.8159$, $n_s = 0.9667$, and $h = 0.6774$.

2.2 Chemical model

We use the publicly available package GRACKLE-3.1.1¹ (Bryan et al. 2014; Smith et al. 2017) to follow thermal and chemical evolution of the collapsing gas. GRACKLE is an open-source chemistry and radiative cooling/heating library suitable for use in numerical astrophysical simulations.

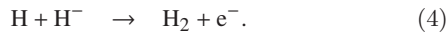
The rate equations of nine chemical species: H, H⁺, He, He⁺, He⁺⁺, e⁻, H⁻, H₂, and H₂⁺ are solved self-consistently along with the hydrodynamics in cosmological simulations. In our simulation, we are using the Haardt & Madau (2012) background spectrum. However, it is known that this background intensity is too weak to reach J_{crit} at $z > 10$ (e.g., Ciardi & Ferrara 2005; Ahn et al. 2009;

¹ <https://grackle.readthedocs.org/>

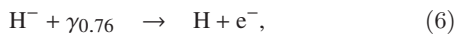
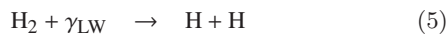
Holzbauer & Furlanetto 2012). The additional local radiation from nearby star formation is considered through the values of k_{H^-} and k_{H_2} in the present work. The treatment of H_2 collisional dissociation by H atom collisions is taken from Martin et al. (1996) and accounts for both the temperature and density dependence of this process. The rate coefficients for the three-body reaction to form H_2 is adopted from Forrey (2013), which produces a flat temperature dependence.

We have assumed a dust-free primordial gas and calculated the radiative cooling and heating rates, accounting for collisional excitation, collisional ionization, free-free transitions, recombination, and photoionization heating, depending on the ionizing radiation field. At very high densities, once the H_2 lines become optically-thick, the decrease in the H_2 cooling rate is accounted for (Ripamonti & Abel 2004). The collision-induced emission cooling of H_2 at high densities is also included (Ripamonti & Abel 2004).

In the direct collapse scenario, a crucial assumption is the suppression of the H_2 formation and cooling. Studies in both semi-analytic analysis and three-dimensional simulations show that a sufficiently strong dissociating Lyman-Werner (LW, 11.2–13.6 eV) flux is required to suppress the H_2 cooling entirely. The main pathway for the formation of H_2 in primordial gas is



In the chemical network, H_2 can be reduced either by photo-dissociation of H_2 or photo-detachment of H^- . Photo-dissociation of the ground state of H_2 happens mostly through absorption in the LW bands to the electronically and vibrationally excited states, and then dissociate to the continuum of the ground state, which is known as the Solomon process (Stecher & Williams 1967). On the other hand, H^- can be photo-detached by photons with energy above 0.76 eV. The chemical reactions are shown as



where γ_{LW} and $\gamma_{0.76}$ represent the photons in the LW bands and the photons with energy above 0.76 eV, respectively. In our work, we perform simulations for a set of H_2 photo-dissociation rate k_{H_2} and H^- photo-detachment rate k_{H^-} , and find the critical conditions for suppression of the H_2 formation.

2.3 Numerical self-shielding approximations

In regions where the LW bands become optically-thick, the photo-dissociation rate and H_2 abundance are much more suppressed. Therefore the cooling rate depends largely on modeling the self-shielding. Usually a self-shielding factor f_{sh} , which is a function of the H_2 column density, N_{H_2} , is adopted to parameterize the H_2 photo-dissociation rate. However, it remains difficult to make an accurate estimate of the self-shielding factor and the H_2 column densities. In 3D simulations, it is computationally expensive to find the exact self-shielding column density along the different directions. Alternatively, a local method is used, which relies on the estimate of N_{H_2} from the local properties of the gas, such

as $N_{\text{H}_2} = n_{\text{H}_2} \lambda$, where n_{H_2} is the H_2 number density, and λ is some characteristic length (e.g. Schaye 2001).

We adopt the improved fitting formula for the self-shielding factor f_{sh} from Wolcott-Green et al. (2011) in our simulations, which is defined as

$$f_{\text{sh}} = \frac{0.965}{(1 + x/b_5)^{1.1}} + \frac{0.035}{(1 + x)^{0.5}} \exp\left[-\frac{(1 + x)^{0.5}}{1180}\right], \quad (7)$$

where $x = N_{\text{H}_2}/5 \times 10^{14} \text{cm}^{-2}$, $b_5 = b/10^5 \text{cm s}^{-1}$ and b is the Doppler parameter. For the N_{H_2} calculation, the improved approximations, e.g., TreeCol algorithm (Clark et al. 2012; Hartwig et al. 2015b,a), six-ray approximation (Yoshida et al. 2007; Glover & Mac Low 2007), or explicit calculation of the column density using HEALPix (Górski et al. 2005; Regan et al. 2016) have been introduced. However, these calculations remain sophisticated and computationally expensive. Instead, we consider three approximations for the characteristic length λ , based on the Jeans length λ_{Jeans} , Sobolev-like length λ_{Sob} , and the reduced Jeans length $\lambda_{\text{Jeans}25} = 0.25 \lambda_{\text{Jeans}}$ proposed by Wolcott-Green et al. (2017). The local Jeans length is defined as $\lambda_{\text{Jeans}} = c_s \sqrt{\pi/(G\rho)}$, where c_s is the sound speed, G is the gravitational constant, and ρ is the gas density. Here $\lambda_{\text{Sob}} = \rho/|\nabla\rho|$ depends on the gas density ρ and its spatial gradient. λ_{Sob} is a method akin to the Sobolev length and is shown in post-processing of 3D simulations to be accurate in the region where $n_{\text{H}_2} < 10^4 \text{cm}^{-3}$ (Gnedin et al. 2009; Wolcott-Green et al. 2011).

3 RESULTS AND DISCUSSION

3.1 The critical curve in the 3D simulations

We have generated the ICs for three chosen haloes. For each halo, we run models applying three different self-shielding approximations, and for each approximation, we have calculated a grid of models in the $k_{\text{H}_2} - k_{\text{H}^-}$ plane. We checked each model for the dominant gas cooling, atomic or H_2 as they evolved.

To examine the effect of H_2 formation, we monitor the gas dynamics of the simulated haloes and check evolution of their thermodynamic parameters, including temperature and density. Models dominated by atomic or H_2 cooling, have a diverging evolution and can be easily distinguished. Fixing the self-shielding approximations and for each k_{H^-} , we found pairs of neighboring models with a dominant atomic and H_2 cooling along the k_{H_2} axis. The transition or critical point lies between these pairs of models. For each k_{H^-} , we have determined the critical points. Thus, we obtained a sequence of critical points which separate the models with atomic and molecular cooling, and which form a critical curve in the $k_{\text{H}^-} - k_{\text{H}_2}$ plane.

As we have discussed in the Introduction, a critical curve in the $k_{\text{H}_2} - k_{\text{H}^-}$ plane can provide a better description for the H_2 suppression (Agarwal et al. 2016; Wolcott-Green et al. 2017). Figure 1 displays our results in the $k_{\text{H}_2} - k_{\text{H}^-}$ plane, for three different haloes. The empty and filled star symbols represent models dominated by molecular and atomic cooling, respectively, using the self-shielding approximation λ_{Jeans} .

Note that models of the same halo and with the same

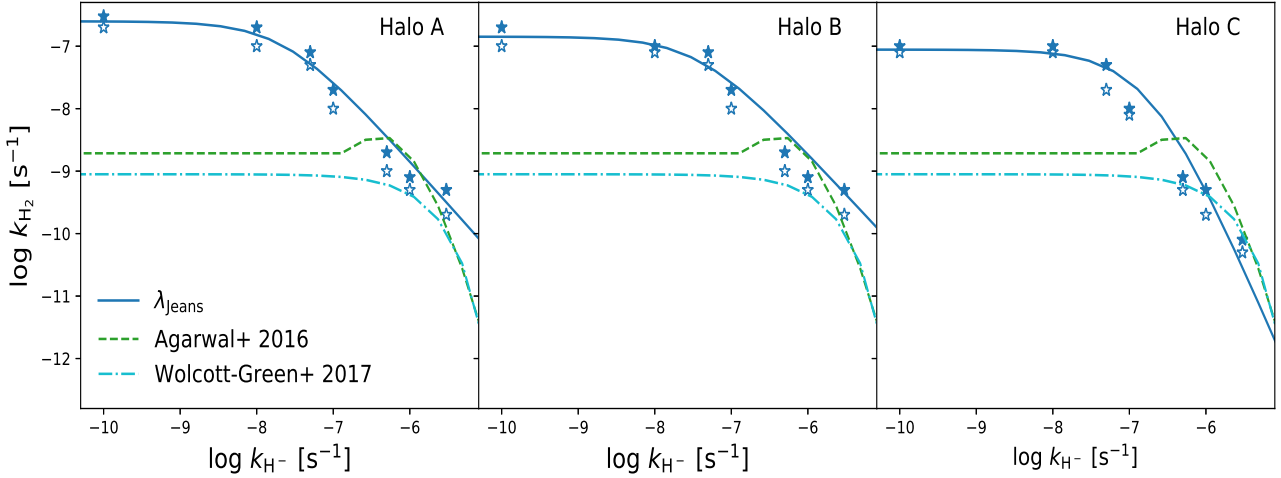


Figure 1. Comparison of the critical curve obtained from 3D simulations (blue solid line) with that from one-zone models. One-zone results from Agarwal et al. (2016) and Wolcott-Green et al. (2017) are shown as green dashed line and cyan dash-dot line, respectively. The green dashed line, as well as our critical blue solid line, are obtained with the same self-shielding approximation λ_{Jeans} , while the cyan dash-dot line has been obtained with λ_{Jeans25} . Each line represents the critical boundary in this parameter space above which the H₂ cooling is prevented in our models, for haloes A, B and C. Empty and filled marks show the dominant H₂ and atomic cooling, respectively, measured in our models. The critical dashed line represents the least square fit to critical points determined by us in the 3D runs.

Table 1. Collapse redshift z_c , dominant cooling Λ , DM virial mass M_v , central gas temperature T_c and the halo cosmological spin parameter λ_{spin} for the simulated haloes, when the maximum refinement level is reached. Here we only list these values for $k_{\text{H}^-} = 10^{-8} \text{ s}^{-1}$. The dominant cooling Λ refers to models slightly above and below the critical curve shown in Figure 1 as filled (H_I) and empty (H₂) symbols, respectively.

	λ	Λ	z_c	M_v	T_c	λ_{spin}
Halo A	λ_{Jeans}	H ₂	17.1	2.5e7	798	0.03
	λ_{Jeans}	H _I	16.8	2.7e7	6217	0.03
	λ_{Jeans25}	H ₂	17.3	2.3e7	871	0.03
	λ_{Jeans25}	H _I	16.8	2.7e7	6159	0.03
	λ_{Sob}	H ₂	17.3	2.3e7	389	0.03
	λ_{Sob}	H _I	16.8	2.7e7	6142	0.03
Halo B	λ_{Jeans}	H ₂	16.7	1.7e7	839	0.01
	λ_{Jeans}	H _I	15.8	2.20e7	6099	0.02
	λ_{Jeans25}	H ₂	18.3	1.2e7	901	0.01
	λ_{Jeans25}	H _I	15.7	2.2e7	6123	0.02
	λ_{Sob}	H ₂	18.0	1.2e7	482	0.00
	λ_{Sob}	H _I	15.8	2.2e7	6087	0.00
Halo C	λ_{Jeans}	H ₂	15.6	2.0e7	874	0.03
	λ_{Jeans}	H _I	16.8	2.7e7	6217	0.03
	λ_{Jeans25}	H ₂	15.7	2.0e7	883	0.03
	λ_{Jeans25}	H _I	14.7	2.5e7	6143	0.03
	λ_{Sob}	H ₂	15.8	1.9e7	831	0.03
	λ_{Sob}	H _I	14.8	2.4e7	6210	0.03

value of k_{H^-} and the shielding parameter λ , which differ only with k_{H_2} will collapse at slightly different redshift. In Table 1, we list the collapse redshifts z_c , DM virial masses M_v , the central gas temperatures T_c , and the halo cosmological spin parameter λ_{spin} , for the selected models, measured when the maximum refinement level is reached. The gas collapse proceeds from inside out and leads to a central runaway, and this runaway occurs after the gas density exceeds the back-

ground DM density (Choi et al. 2013, 2015; Shlosman et al. 2016). The collapse proceeds very rapidly, and the maximum refinement level is reached only in about a few million years (Luo et al. 2016). We stop the simulations when the maximum refinement level has been reached, and measure the required parameters in Table 1. These are listed for different λ approximations and the dominant cooling mechanisms for each approximation. Only models with $k_{\text{H}^-} = 10^{-8} \text{ s}^{-1}$ are shown in this Table, for simplicity.

In Table 1, models dominated by atomic cooling, i.e., models with k_{H_2} above the critical value, collapse with a slight delay compared to a corresponding model with molecular cooling below the critical point. For all models, the collapse redshifts range from 17 to 13, and the virial masses are approximately a few times $10^7 M_\odot$. In the H₂ cooling models, the central gas temperature drops down to a few $\times 100$ K, while in the atomic cooling models, the temperature remains roughly constant, around 6,000 K.

For a given k_{H^-} , the H₂ formation is gradually inhibited with increasing k_{H_2} . After determining the critical points for each k_{H^-} , we perform the least-square fit and find that the fitting formula can be approximated by

$$k_{\text{H}_2} = a \left(1 + \frac{k_{\text{H}^-}}{b} \right)^c. \quad (8)$$

The fitting parameters have been listed in Table 2. In Figure 1, for each halo, we display the fitted critical curve in blue solid line with the self-shielding approximation λ_{Jeans} . Moreover, we have added the critical curve from Agarwal et al. (2016) (green dashed line), which has been calculated with the one-zone ENZO code, using the same self-shielding approximation λ_{Jeans} , and the same cooling package GRACKLE described in Section 2.2.

Comparison with the critical curve obtained from the one-zone simulations of Agarwal et al. (2016) and that from our 3D simulations under otherwise similar conditions, yields a substantial difference between them, up to two orders of

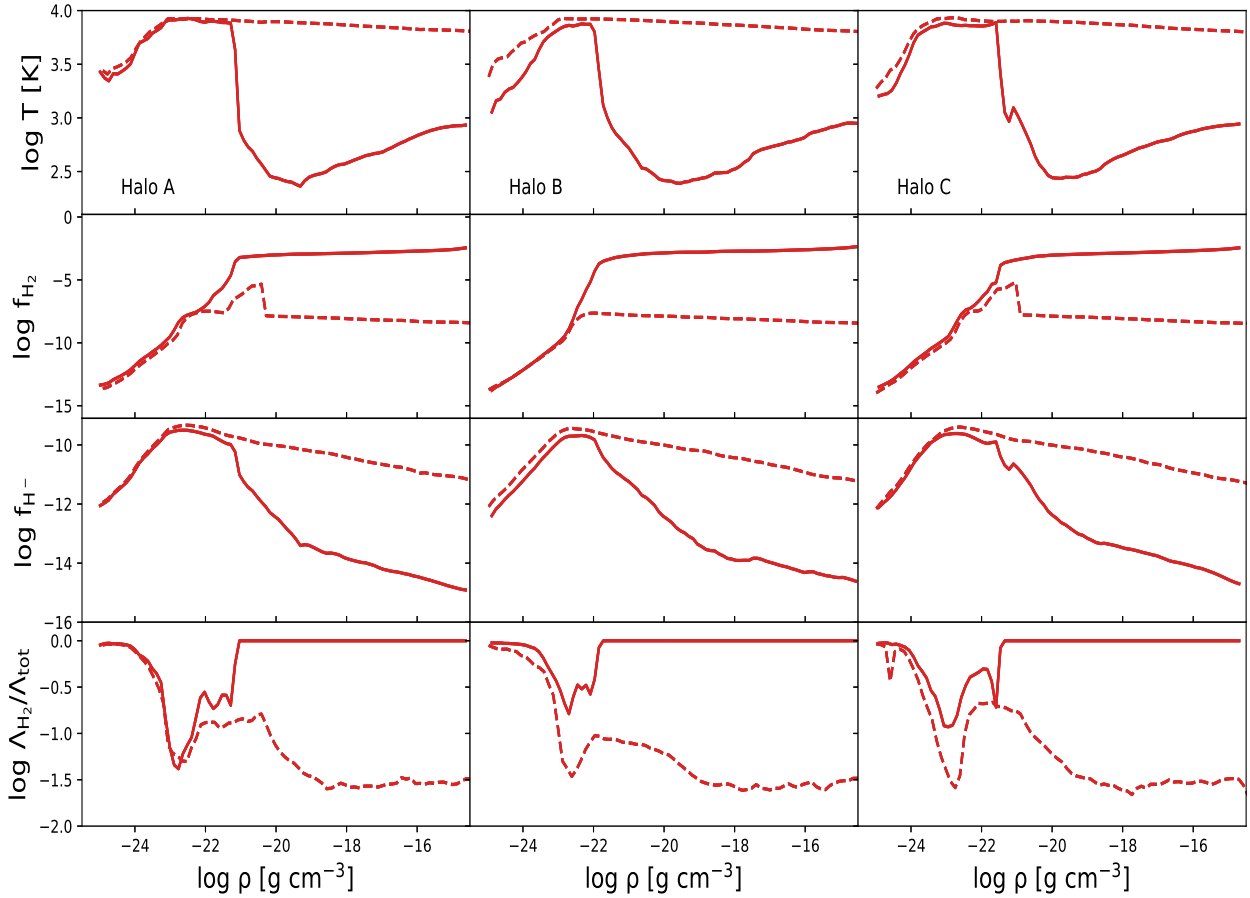


Figure 2. Profiles of the gas temperature, of the H₂ and H⁻ fractions, and the ratios of the molecular to the total cooling rates as a function of the gas density. Only profiles under the condition of $k_{\text{H}^-} = 10^{-8} \text{ s}^{-1}$ are shown. The curves represent realizations with $\lambda_{\text{Jeans}25}$ approximation, where the solid lines represent the collapse with the dominant H₂ cooling and the dashed lines represent the collapse with the atomic cooling.

magnitude. Furthermore, we have added additional curve (cyan dash-dot line) in Figure 1 from Wolcott-Green et al. (2017) which has been obtained from one-zone simulations using the cooling package similar to Shang et al. (2010) and the self-shielding parameter $\lambda_{\text{Jeans}25}$. We find the difference between the 3D and one-zone simulations is significant for $k_{\text{H}^-} < 10^{-7} \text{ s}^{-1}$. In the vicinity of $k_{\text{H}^-} \sim 10^{-6} \text{ s}^{-1}$, the difference minimizes, and then increases again for higher values of k_{H^-} . Therefore, the J_{crit} value based on one-zone results could be underestimated (see Section 3.3 for the J_{crit} calculations). Our results indicate that to suppress the H₂ cooling, requires a higher LW flux for the same k_{H^-} rate.

Where exactly the evolution of our models with atomic and molecular cooling bifurcates? Why do models based on the 3D simulations differ profoundly from those in one-zone? We discuss the details of this diverging evolution in the following sections.

3.2 Impact of the self-shielding column density

Evolution of direct collapse models depends strongly on the dominant cooling mechanism, which affects their temperature profiles and other thermodynamic parameters. Figure 2 exhibits the profiles of the gas temperature, the H₂ fraction

f_{H_2} , the H⁻ fraction f_{H^-} , and the ratios of the molecular to the total cooling rates, as functions of the gas density, for the self-shielding parameter $\lambda_{\text{Jeans}25}$. Additional approximations, λ_{Jeans} and λ_{Sob} , have been evolved as well, but are not shown here. The solid lines show the collapse dominated by the molecular cooling, and the dashed lines correspond to the dominant atomic cooling.

At the initial stage of the collapse, the gas basically goes into the free-fall, and is shock-heated to the halo virial temperature of $\sim 10^4 \text{ K}$ around the density of $\sim 10^{-24} \text{ g cm}^{-3}$ at the virial radius. When the gas density reaches about $10^{-23} \text{ g cm}^{-3}$, the H₂ formation becomes important for the future evolution of the gas. However, for higher k_{H_2} , the photo-dissociation will suppress the H₂ formation. Hence, the gas still follows the atomic cooling and the collapse proceeds isothermally. The temperature stays nearly constant around 6,000 K, and the H₂ fraction is kept around its the maximum value of 10^{-8} only.

As the gas flows inwards, it remains largely neutral, and the already small H⁻ fraction is slightly decreasing with an increasing density. This is the result of a decreasing fraction of the free electrons required for the H⁻ formation. In cases with the H₂ cooling being dominant, the total gas cooling rate increases dramatically, causing a substantial

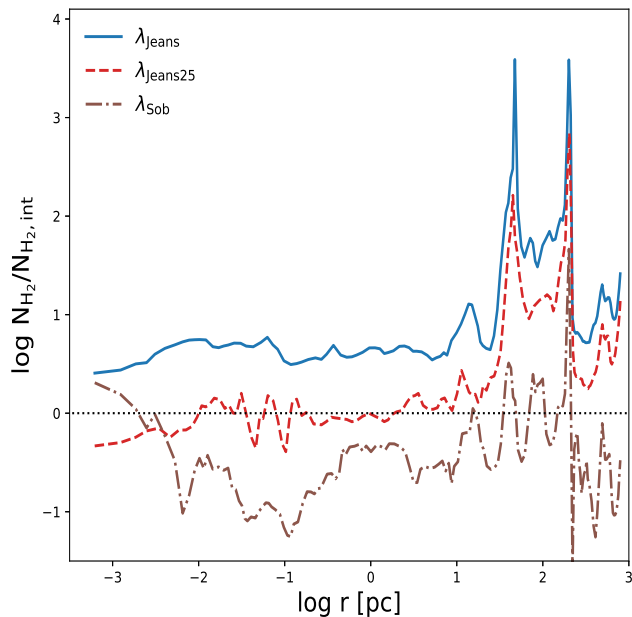


Figure 3. Comparison between the column density approximations for halo A. The ratios of the H₂ column density N_{H_2} to the actual column density $N_{\text{H}_2,\text{int}}$ are displayed. Approximations for λ_{Jeans} , λ_{Jeans25} and λ_{Sob} , are shown as the blue solid, red dashed, and brown dash-dot lines, respectively. The black dotted line is drawn to delineate the ratio of unity.

drop in the gas temperature, the electron and H⁻ fractions. Around $10^{-18} \text{ g cm}^{-3}$, the collisional dissociation of H₂ begins to suppress the H₂ cooling. However, the inflow still does not generate the high density/high temperature regime, the so-called ‘zone of no return’ (Inayoshi & Omukai 2012; Fernandez et al. 2014). The compressional heating rate of the collapsing gas decreases substantially due to a lower accretion rate, \dot{M} , and the sound speed, c_s — these are related simply by $\dot{M} \sim c_s^3/G$. So the heating-cooling balance in the collapsing gas remains at the much lower temperature of the molecular gas.

As we have discussed in the section 2.3, the primordial gas cooling rate within a DM halo depends on the self-shielding effect of H₂. The gas column densities in our models have been calculated using the λ_{Jeans} , λ_{Jeans25} and λ_{Sob} approximations. In the next step, we test the accuracy of approximating these column densities, N_{H_2} . For comparison, we have calculated the actual column density by integrating the H₂ profile from the outside inwards, and compared it with column densities obtained from λ_{Jeans} , λ_{Jeans25} and λ_{Sob} approximations.

In Figure 3, we present ratios of the column densities N_{H_2} from the adopted self-shielding approximation to that calculated from integrating the H₂ number density profile. The ratio which stays closer to unity, reflects the more accurate approximation. We display our results for the simulated halo A in the atomic cooling regimes, for fixed $k_{\text{H}^-} = 10^{-8} \text{ s}^{-1}$. In this Figure, we only show the results of integration along a single radial sightline in the direction away from the halo center. Results for all three haloes, and for each halo toward different sightlines are qualitatively sim-

Table 2. Least-square fitting parameters for the critical curves determined from 3D numerical simulations presented in this work (see eq.7).

	λ	a	b	c
Halo A	λ_{Jeans}	2.5e-07	2.4e-08	-1.4
	λ_{Jeans25}	3.1e-08	1.2e-08	-1.6
	λ_{Sob}	1.1e-10	1.2e-07	-1.9
Halo B	λ_{Jeans}	1.4e-07	3.9e-08	-1.3
	λ_{Jeans25}	3.2e-08	1.3e-07	-1.6
	λ_{Sob}	1.1e-10	1.1e-07	-2.0
Halo C	λ_{Jeans}	8.8e-08	1.9e-07	-2.9
	λ_{Jeans25}	3.2e-08	3.1e-07	-3.1
	λ_{Sob}	1.2e-10	1.0e-07	-2.0

ilar, and so haloes B and C have been omitted from this Figure. Within the central ~ 10 pc, the λ_{Jeans} approximation gives a higher estimate of N_{H_2} by a factor of 4, while usage of λ_{Sob} leads to the estimate which is too low. The λ_{Sob} method also shows a relatively large scatter along the radius. However, the ratio obtained from λ_{Jeans25} to that determined from simulations lies much closer to unity, within a factor of 2 at radius smaller than 10 pc. We find the λ_{Jeans25} approximation provides a more accurate estimate of the H₂ self-shielding.

The self-shielding factors f_{sh} for halo A along a single sightline are plotted in Figure 4 for the three approximations, λ_{Jeans} , λ_{Jeans25} and λ_{Sob} , from left to right, respectively. The solid lines represent the f_{sh} in the H₂ cooling cases, and the dashed lines in the atomic cooling cases. Outside the central ~ 10 pc region of the collapse, f_{sh} is insensitive to the choice of λ . But within the central 10 pc, the H₂ fraction is sharply increasing (see the second row of Figure 2), and the λ approximation becomes important for the f_{sh} calculation.

Finally, we compared the critical curves calculated in the $k_{\text{H}^-} - k_{\text{H}_2}$ plane with three different prescriptions for the self-shielding (Figure 5). This has been performed for each of the three DM haloes. The fitted curves are given in blue solid, red dashed and brown dash-dot lines for λ_{Jeans} (see also Figure 1), λ_{Jeans25} and λ_{Sob} , respectively. The least-square fitting parameters have been listed in Table 2.

The critical curve for λ_{Jeans} shows that it lies consistently above that the critical curve for λ_{Sob} . So the required radiation intensity to suppress the H₂ formation, therefore, should be stronger as well, which means the required LW radiation intensity is higher for a given k_{H^-} . The critical curve is sensitive, by about one order of magnitude, to the choice of the column density approximation used, especially for $k_{\text{H}^-} < 10^{-7} \text{ s}^{-1}$. For $k_{\text{H}^-} > 10^{-7} \text{ s}^{-1}$, the curve drops down sharply, because H⁻ photo-detachment becomes the dominant mechanism for the suppression of H₂ abundance and thus the curve is insensitive to the LW rate k_{H_2} . We do not adopt the fitting formula given by the one-zone simulations of Wolcott-Green et al. (2017) and Agarwal et al. (2016), which fit the critical curve with an exponential tail at higher k_{H^-} . In fact we find that the decay is better fit by a power-law shape, with an index of about -1.6. The reason for this is that in the 3D simulations, the spatial variations in the temperature and density within the accretion flow (e.g., Shang et al. 2010), or the hydrodynamic effects (e.g.,

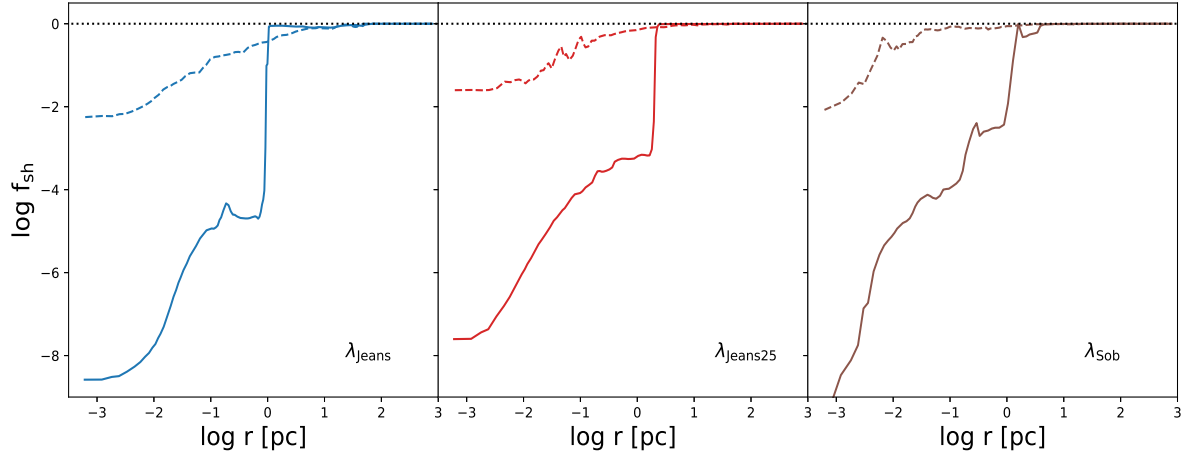


Figure 4. Profiles of the self-shielding factor as functions of radius for the simulated halo A at fixed $k_{\text{H}^-} = 10^{-8} \text{ s}^{-1}$. The solid lines represent the collapse with the dominant H_2 cooling and the dashed lines represent the collapse with the dominant atomic cooling. From the left to the right panels, approximations for λ_{Jeans} , λ_{Jeans25} and λ_{Sob} , are shown as blue, red, and brown lines, respectively. The black dotted line is drawn to delineate the ratio of unity.

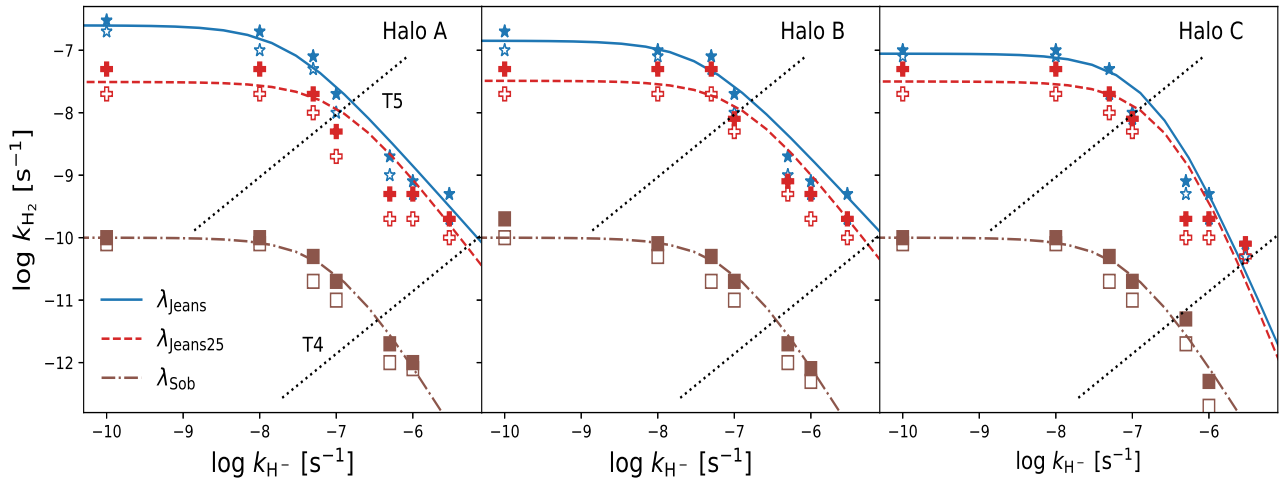


Figure 5. The critical curves in the $k_{\text{H}_2} - k_{\text{H}^-}$ plane (see caption for Figure 1), using three different methods to calculate the self-shielding characteristic length λ ; namely, λ_{Jeans} (blue solid line, shown also in Fig. 1), λ_{Jeans25} (red dashed line), and λ_{Sob} (brown dash-dot line). The two diagonal black dotted lines represent the rates with varying intensity for the T4 (lower) and T5 spectrum (upper), respectively.

Latif et al. 2014) will enhance the H_2 formation from H^- . This is a crucial difference between the one-zone and 3D simulations.

3.3 Calculation of J_{crit} from the critical curve

In Figure 5, the two diagonal dotted lines illustrate the relationship between k_{H_2} and k_{H^-} with varying intensity for a T4 (lower) and T5 (upper) spectral shapes, respectively. We are able to reproduce the critical intensity J_{crit} obtained in previous studies by assuming their fixed blackbody spectral shapes. The critical values lie at the intersection of the diagonal dotted lines crossing the critical curves.

In Table 3, we list the critical intensity J_{crit} for a blackbody spectra of T5 and T4, adopted from previous studies. The second column of Table 3 displays the self-shielding λ approximation adopted in these studies. The third and fourth columns show J_{crit} by assuming a T5 (lower) and T4

(upper) spectral shapes, respectively. The last two columns show the numerical methods used, as well as the methods applied for the self-shielding factor estimates. We have reproduced the calculations of J_{crit} . Those lie at the intersections of the diagonal dotted lines with the critical curves shown in Figures 1 and 5. The values of J_{crit} reproduced from the previous one-zone simulations by Wolcott-Green et al. (2017) and Agarwal et al. (2016) are also shown in the Table as a comparison.

We have obtained J_{crit} from our three simulated haloes. The value of J_{crit} varies from halo to halo, but the variations are within a factor of two. This is shown as a range of values in Table 3. By comparing J_{crit} calculated in 3D simulations applying the λ_{Jeans} approximation, our J_{crit} with T5 is consistent with that from Shang et al. (2010). It is about 30% higher in comparison with Hartwig et al. (2015a). Our J_{crit} with T4 is consistent with that from Shang et al. (2010),

Table 3. Compilations of J_{crit} values in units of $J_{\text{LW},21}$ in earlier works using the T5 or T4 black-body spectra. The critical values are obtained at the intersection of the diagonal dotted lines with the critical curves shown in Figures 1 and 5. The last column lists the method used for the self-shielding approximation.

Authors	λ	J_{crit,T_5}	J_{crit,T_4}	Methods	Approximations
This Work	λ_{Jeans}	1e4-2e4	13-42	3D	Wolcott-Green et al. (2011)
	$\lambda_{\text{Jeans}25}$	7e3-8e3	13-27	3D	Wolcott-Green et al. (2011)
	λ_{Sob}	75-82	1.6-1.9	3D	Wolcott-Green et al. (2011)
Shang et al. (2010)	λ_{Jeans}	1.2e4	39	one-zone	Draine & Bertoldi (1996)
Shang et al. (2010)	λ_{Jeans}	1e4-1e5	30-300	3D	Draine & Bertoldi (1996)
Latif et al. (2014)	--	--	400-1500	3D	Wolcott-Green et al. (2011)
Latif et al. (2014)	--	--	30-40	one-zone	Wolcott-Green et al. (2011)
Sugimura et al. (2014)	λ_{Jeans}	1.4e3	59.8	one-zone	Wolcott-Green et al. (2011)
Hartwig et al. (2015a)	λ_{Jeans}	3.5e3-5.5e3	--	3D	Wolcott-Green et al. (2011)
Agarwal et al. (2016)	λ_{Jeans}	1.5e3	19.4	one-zone	Wolcott-Green et al. (2011)
Wolcott-Green et al. (2017)	$\lambda_{\text{Jeans}25}$	6.6e2	19.3	one-zone	Wolcott-Green et al. (2011)

but is smaller by one order of magnitude with that from Latif et al. (2014).

Using different λ approximation, the values of J_{crit} differ by up to two orders of magnitude. In our calculations, the J_{crit} in λ_{Sob} approximation is smaller than that in λ_{Jeans} by almost two orders of magnitude. In addition, for a softer spectrum, e.g., T4, the values of J_{crit} are smaller than the values derived from a harder spectrum with T5, again by up to two orders of magnitude. For the softer spectrum, the radiation field above 0.76 eV lead to an increase in k_{H^-} . With increasing k_{H^-} , the required k_{H_2} or J_{crit} to suppress the H₂ cooling decreases.

Intensities estimated from our 3D simulations tend to be larger compared to those obtained in one-zone simulations. For example, the values of J_{crit,T_5} from one-zone simulations by Sugimura et al. (2014) and Agarwal et al. (2016) are one order of magnitude smaller than those calculated from 3D simulations by Shang et al. (2010) and by our work. The difference in J_{crit} between the one-zone and 3D simulations has been also found by Hartwig et al. (2015a) and Latif et al. (2014), who used the single-temperature blackbody spectral shape.

Previous studies which obtained J_{crit} , used the single-temperature blackbody spectra. Consequently, these studies obtained only a single point each on the $k_{\text{H}_2} - k_{\text{H}^-}$ plane. By comparing J_{crit} obtained from previous studies with our values from the critical curve, we find the critical curve provides a more general and compelling way to determine the critical intensity. The single blackbody results from previous works have been reproduced using this curve.

4 DISCUSSION AND CONCLUDING REMARKS

We have calculated the conditions for suppressing the formation of H₂ in the direct collapse scenario towards the SMBH seeds, within DM haloes. Using series of 3D numerical simulations we have obtained the critical intensity of the background UV radiation by constructing the critical curves in the $k_{\text{H}_2} - k_{\text{H}^-}$ parameter plane, separating models with dominant atomic and molecular cooling. We have also shown the dependence of the critical conditions on the choice of the H₂

column density approximation in the self-shielding calculation. Our main findings can be summarized as follows.

- We have verified that there exists a critical curve in the $k_{\text{H}_2} - k_{\text{H}^-}$ parameter plane, above which the H₂ cooling is suppressed, and the atomic cooling dominates.
- We have provided a fitting formula for this critical curve and found that the fitted curve based on the 3D numerical simulations differs substantially from that obtained in the one-zone simulations, both in its position in the $k_{\text{H}_2} - k_{\text{H}^-}$ parameter plane and in its shape.
- We have compared the critical curves calculated in 3D simulations using three different H₂ column density approximations in the self-shielding calculation, λ_{Jeans} , $\lambda_{\text{Jeans}25}$ and λ_{Sob} . These approximations correspond to the Jeans length, a fraction of the Jeans length and the Sobolev length, respectively. We find that the characteristic lengthscale for shielding can be improved by using $\lambda_{\text{Jeans}25}$, which is four times smaller than the local Jeans length.

The direct collapse models involve the gas accretion within the DM haloes, resulting in the SMBH seeds of $\sim 10^4 - 10^6 M_{\odot}$. It circumvents the difficulties associated with the growth of the Pop III black hole remnants from stellar masses to the SMBH masses found in the galactic centers.

To sustain a high inflow rate of $\sim 0.1 - 1 M_{\odot} \text{ yr}^{-1}$, the H₂ formation should be inhibited in the primordial gas. To prevent accretion flow fragmentation induced by the H₂ cooling, the halo must be exposed to the background UV radiation whose intensity exceeds J_{crit} . To obtain the J_{crit} , typically, a single blackbody or power-law spectra have been assumed in the literature to model the background radiation. However in realistic situations, this radiation field is time-dependent, and a simple spectral shape model cannot capture all the intricacies associated with the flux variability, anisotropy and changing spectral shape. Therefore, it is advantageous to use an alternative approach and deal with the critical intensity that is defined in a more general way, by a combination of k_{H_2} and k_{H^-} . There is no need to make any initial assumptions on the properties of the underlying radiation.

We have tested this approach in the fully 3D simulations, and found that a critical curve can exist in the $k_{\text{H}_2} - k_{\text{H}^-}$ parameter plane. The critical curve position and shape is strongly affected by replacing the one-zone with

more realistic simulations in the 3D. Moreover, we have successfully applied a new fitting formula to the critical curve in this parameter space, and compared this curve to those obtained in the one-zone simulations. The main outcome of this comparison is that the critical curve in the 3D simulations lies substantially higher than that from the one-zone simulations, and the required LW flux is higher by up to two orders of magnitude for the same rate k_{H} .

Our analysis also includes the H_2 column density approximations for the self-shielding factor calculation. As the gas flows inwards, its density increases, and so is the H_2 number density. When the H_2 column densities increase (e.g., $N_{\text{H}_2} > 10^{14} \text{ cm}^{-2}$), the photo-dissociation is suppressed because the region becomes optically-thick for the Lyman-Werner photons. The treatment of the gas cooling, therefore, depends on the H_2 self-shielding approximation. The three cases considered here, λ_{Jeans} , $\lambda_{\text{Jeans}25}$, and λ_{Sob} , which approximate the characteristic length, provide the column densities, some of which differ from the actual column densities estimated directly from the simulations. The λ_{Jeans} approximation overestimates the shielding, while the λ_{Sob} approximation significantly underestimates it. We find that $\lambda_{\text{Jeans}25}$ suggested by Wolcott-Green et al. (2017) yields the most accurate approach to the true characteristic self-shielding.

In summary, the 3D simulations in tandem with the $\lambda_{\text{Jeans}25}$ approximation for the column density, provide a substantial improvement over the one-zone simulation with fixed spectral shapes of the background UV radiation.

ACKNOWLEDGEMENTS

We thank the Enzo and YT support team for help. All the analysis has been conducted using yt (Turk et al. 2011), <http://yt-project.org/>. Y.L. acknowledges the support from NSFC grant No. 11903026. This work has been partially supported by the Hubble Theory grant HST-AR-14584 (to I.S.), and by JSPS KAKENHI grant 16H02163 (to I.S.) and 17H01111 (to K.N.). I.S. and K.N. are grateful for a generous support from the International Joint Research Promotion Program at Osaka University. The STScI is operated by the AURA, Inc., under NASA contract NAS5-26555. T.F. acknowledges the support from the National Key R&D Program of China No. 2017YFA0402600, and NSFC grants No. 11525312, 11890692. Numerical simulations have been performed on Tianhe-2 at the National Supercomputer Center in Guangzhou, on Supercomputer at the Shanghai Astronomical Observatory, as well as on the LCC Linux Cluster of the University of Kentucky.

REFERENCES

Abel T., Anninos P., Zhang Y., Norman M. L., 1997, *New Astron.*, **2**, 181
 Agarwal B., Khochfar S., Johnson J. L., Neistein E., Dalla Vecchia C., Livio M., 2012, *MNRAS*, **425**, 2854
 Agarwal B., Smith B., Glover S., Natarajan P., Khochfar S., 2016, *MNRAS*, **459**, 4209
 Ahn K., Shapiro P. R., Iliev I. T., Mellema G., Pen U.-L., 2009, *ApJ*, **695**, 1430
 Ardaneh K., Luo Y., Shlosman I., Nagamine K., Wise J. H., Begelman M. C., 2018, *MNRAS*, **479**, 2277

Bañados E., et al., 2018, *Nature*, **553**, 473
 Begelman M. C., 2010, *MNRAS*, **402**, 673
 Begelman M. C., Rees M. J., 1978, *MNRAS*, **185**, 847
 Begelman M. C., Shlosman I., 2009, *ApJ*, **702**, L5
 Begelman M. C., Volonteri M., Rees M. J., 2006, *MNRAS*, **370**, 289
 Bromm V., Loeb A., 2003, *ApJ*, **596**, 34
 Bryan G. L., Norman M. L., 1997, in Clarke D. A., West M. J., eds, *Astronomical Society of the Pacific Conference Series Vol. 12, Computational Astrophysics; 12th Kingston Meeting on Theoretical Astrophysics*. p. 363 ([arXiv:astro-ph/9710186](https://arxiv.org/abs/astro-ph/9710186))
 Bryan G. L., Norman M. L., Stone J. M., Cen R., Ostriker J. P., 1995, *Computer Physics Communications*, **89**, 149
 Bryan G. L., et al., 2014, *The Astrophysical Journal Supplement Series*, **211**, 19
 Choi J.-H., Shlosman I., Begelman M. C., 2013, *ApJ*, **774**, 149
 Choi J.-H., Shlosman I., Begelman M. C., 2015, *MNRAS*, **450**, 4411
 Chon S., Latif M. A., 2017, *MNRAS*, **467**, 4293
 Ciardi B., Ferrara A., 2005, *Space Sci. Rev.*, **116**, 625
 Ciardi B., Ferrara A., Abel T., 2000, *ApJ*, **533**, 594
 Clark P. C., Glover S. C. O., Klessen R. S., 2012, *MNRAS*, **420**, 745
 Colella P., Woodward P. R., 1984, *Journal of Computational Physics*, **54**, 174
 Dijkstra M., Haiman Z., Mesinger A., Wyithe J. S. B., 2008, *MNRAS*, **391**, 1961
 Dijkstra M., Ferrara A., Mesinger A., 2014, *MNRAS*, **442**, 2036
 Draine B. T., Bertoldi F., 1996, *ApJ*, **468**, 269
 Dunn G., Bellovary J., Holley-Bockelmann K., Christensen C., Quinn T., 2018, *ApJ*, **861**, 39
 Eisenstein D. J., Hut P., 1998, *ApJ*, **498**, 137
 Fan X., et al., 2003, *AJ*, **125**, 1649
 Fernandez R., Bryan G. L., Haiman Z., Li M., 2014, *MNRAS*, **439**, 3798
 Forrey R. C., 2013, *ApJ*, **773**, L25
 Ge Q., Wise J. H., 2017, *MNRAS*, **472**, 2773
 Glover S. C. O., 2015a, *MNRAS*, **451**, 2082
 Glover S. C. O., 2015b, *MNRAS*, **453**, 2901
 Glover S. C. O., 2016, arXiv e-prints, p. [arXiv:1610.05679](https://arxiv.org/abs/1610.05679)
 Glover S. C. O., Jappsen A. K., 2007, *ApJ*, **666**, 1
 Glover S. C. O., Mac Low M.-M., 2007, *ApJS*, **169**, 239
 Gnedin N. Y., Tassis K., Kravtsov A. V., 2009, *ApJ*, **697**, 55
 Górski K. M., Hivon E., Banday A. J., Wand elt B. D., Hansen F. K., Reinecke M., Bartelmann M., 2005, *ApJ*, **622**, 759
 Greif T. H., Johnson J. L., Bromm V., Klessen R. S., 2007, *ApJ*, **670**, 1
 Greif T. H., Springel V., White S. D. M., Glover S. C. O., Clark P. C., Smith R. J., Klessen R. S., Bromm V., 2011, *ApJ*, **737**, 75
 Haardt F., Madau P., 2012, *ApJ*, **746**, 125
 Habouzit M., Volonteri M., Latif M., Dubois Y., Peirani S., 2016, *MNRAS*, **463**, 529
 Haehnelt M. G., Rees M. J., 1993, *MNRAS*, **263**, 168
 Hahn O., Abel T., 2011, *MNRAS*, **415**, 2101
 Haiman Z., Abel T., Rees M. J., 2000, *ApJ*, **534**, 11
 Hartwig T., Glover S. C. O., Klessen R. S., Latif M. A., Volonteri M., 2015a, *MNRAS*, **452**, 1233
 Hartwig T., Clark P. C., Glover S. C. O., Klessen R. S., Sasaki M., 2015b, *ApJ*, **799**, 114
 Holzbauer L. N., Furlanetto S. R., 2012, *MNRAS*, **419**, 718
 Inayoshi K., Haiman Z., 2014, *MNRAS*, **445**, 1549
 Inayoshi K., Omukai K., 2012, *MNRAS*, **422**, 2539
 Inayoshi K., Tanaka T. L., 2015, *MNRAS*, **450**, 4350
 Inoue A. K., 2011, *MNRAS*, **415**, 2920
 Johnson J. L., Dijkstra M., 2017, *A&A*, **601**, A138
 Koushiappas S. M., Bullock J. S., Dekel A., 2004, *MNRAS*, **354**, 292

- Latif M. A., Schleicher D. R. G., Schmidt W., Niemeyer J., 2013, *MNRAS*, **433**, 1607
- Latif M. A., Bovino S., Van Borm C., Grassi T., Schleicher D. R. G., Spaans M., 2014, *MNRAS*, **443**, 1979
- Latif M. A., Bovino S., Grassi T., Schleicher D. R. G., Spaans M., 2015, *MNRAS*, **446**, 3163
- Latif M. A., Omukai K., Habouzit M., Schleicher D. R. G., Volonteri M., 2016, *ApJ*, **823**, 40
- Leitherer C., et al., 1999, *ApJS*, **123**, 3
- Li J., Cao X., 2019, arXiv e-prints, p. [arXiv:1910.03744](https://arxiv.org/abs/1910.03744)
- Loeb A., Rasio F. A., 1994, *ApJ*, **432**, 52
- Luo Y., Nagamine K., Shlosman I., 2016, *MNRAS*, **459**, 3217
- Luo Y., Ardaneh K., Shlosman I., Nagamine K., Wise J. H., Begelman M. C., 2018, *MNRAS*, **476**, 3523
- Lupi A., Colpi M., Devecchi B., Galanti G., Volonteri M., 2014, *MNRAS*, **442**, 3616
- Lupi A., Haardt F., Dotti M., Fiacconi D., Mayer L., Madau P., 2016, *MNRAS*, **456**, 2993
- Madau P., Haardt F., Dotti M., 2014, *ApJ*, **784**, L38
- Maio U., Borgani S., Ciardi B., Petkova M., 2019, *Publ. Astron. Soc. Australia*, **36**, e020
- Martin P. G., Schwarz D. H., Mandy M. E., 1996, *ApJ*, **461**, 265
- Miyake S., Stancil P. C., Sadehghpour H. R., Dalgarno A., McLaughlin B. M., Forrey R. C., 2010, *ApJ*, **709**, L168
- Mortlock D. J., et al., 2011, *Nature*, **474**, 616
- Norman M. L., Bryan G. L., 1999, in Miyama S. M., Tomisaka K., Hanawa T., eds, *Astrophysics and Space Science Library Vol. 240, Numerical Astrophysics*. p. 19 ([arXiv:astro-ph/9807121](https://arxiv.org/abs/astro-ph/9807121)), doi:10.1007/978-94-011-4780-4_3
- Omukai K., 2001, *ApJ*, **546**, 635
- Planck Collaboration et al., 2016, *A&A*, **594**, A13
- Rees M. J., 1984, *ARA&A*, **22**, 471
- Regan J. A., Haehnelt M. G., 2009, *MNRAS*, **396**, 343
- Regan J. A., Johansson P. H., Wise J. H., 2016, *MNRAS*, **459**, 3377
- Ripamonti E., Abel T., 2004, *MNRAS*, **348**, 1019
- Schaerer D., 2003, *A&A*, **397**, 527
- Schaye J., 2001, *ApJ*, **562**, L95
- Schleicher D. R. G., Spaans M., Glover S. C. O., 2010, *ApJ*, **712**, L69
- Shang C., Bryan G. L., Haiman Z., 2010, *MNRAS*, **402**, 1249
- Shapiro S. L., Teukolsky S. A., 1985, *ApJ*, **298**, 58
- Shlosman I., Choi J.-H., Begelman M. C., Nagamine K., 2016, *MNRAS*, **456**, 500
- Smith B. D., et al., 2017, *MNRAS*, **466**, 2217
- Stecher T. P., Williams D. A., 1967, *ApJ*, **149**, L29
- Sugimura K., Omukai K., Inoue A. K., 2014, *MNRAS*, **445**, 544
- Tanaka T., Haiman Z., 2009, *ApJ*, **696**, 1798
- Truelove J. K., Klein R. I., McKee C. F., Holliman John H. I., Howell L. H., Greenough J. A., 1997, *ApJ*, **489**, L179
- Turk M. J., Smith B. D., Oishi J. S., Skory S., Skillman S. W., Abel T., Norman M. L., 2011, *The Astrophysical Journal Supplement Series*, **192**, 9
- Venemans B. P., et al., 2017, *ApJ*, **851**, L8
- Visbal E., Haiman Z., Bryan G. L., 2014, *MNRAS*, **445**, 1056
- Visbal E., Haiman Z., Bryan G. L., 2015, *MNRAS*, **453**, 4456
- Volonteri M., Rees M. J., 2006, *ApJ*, **650**, 669
- Willott C. J., et al., 2010, *AJ*, **139**, 906
- Wise J. H., Abel T., 2008, *ApJ*, **685**, 40
- Wolcott-Green J., Haiman Z., Bryan G. L., 2011, *MNRAS*, **418**, 838
- Wolcott-Green J., Haiman Z., Bryan G. L., 2017, *MNRAS*, **469**, 3329
- Wu X.-B., et al., 2015, *Nature*, **518**, 512
- Yoshida N., Oh S. P., Kitayama T., Hernquist L., 2007, *ApJ*, **663**, 687
- Yue B., Ferrara A., Salvaterra R., Xu Y., Chen X., 2013, *MNRAS*, **433**, 1556
- Yue B., Ferrara A., Salvaterra R., Xu Y., Chen X., 2014, *MNRAS*, **440**, 1263
- Yue B., Ferrara A., Pacucci F., Omukai K., 2017, *ApJ*, **838**, 111
- Zel'dovich Y. B., Podurets M. A., 1965, *Azh*, **42**, 963

This paper has been typeset from a $\text{\TeX}/\text{\LaTeX}$ file prepared by the author.